Grazing incidence broad ion beams for reducing line-edge roughness

2010 J. Micromech. Microeng. 20 075038

(http://iopscience.iop.org/0960-1317/20/7/075038)

J. Micromech. Microeng. **20** (2010) 075038 (6pp) doi:10.1088/0960-1317/20/7/075038

Grazing incidence broad ion beams for reducing line-edge roughness

C R M Struck[1], R Flauta[1], M J Neumann[1], K N Kim[1], R Raju[1], R L Bristol[2] and D N Ruzic[1]

[1] Center for Plasma-Material Interactions, University of Illinois at Urbana-Champaign,Urbana, IL 61801, USA
[2] Intel Corporation, Components Research, Hillsboro, OR 97124, USA

E-mail: druzic@illinois.edu

Received 24 February 2010, in final form 11 May 2010
Published 28 June 2010
Online at stacks.iop.org/JMM/20/075038

Abstract
As semiconductor feature sizes continue to decrease, the phenomena of line-edge roughness (LER) becomes more disruptive in chip manufacturing. While many efforts are underway to decrease LER from the photoresist, post-developed smoothing techniques may be required to continue shrinking chip features economically. This paper reports on one such method employing the use of a broad ion beam at grazing incidence along the features. This method smooths relatively long spatial-length LER, a potential advantage over other smoothing techniques that focus on just molecular-scale LER. LER reduction numbers using Ne and Ar beams are reported at both short and long spatial wavelengths. Variables include beam energy, length of time and angular dependence. LER measurements are taken using the Hitachi image-analysis software on top–down analytical scanning electron microscope (SEM) measurements. Line-profile data are taken from cross-sectional SEM photographs. Tests have achieved a reduction in LER from 9.8 ± 0.67 nm to 5.5 ± 0.86 nm for 45 nm critical dimensions using an Ar beam at 500 eV for 6 s at an 85° angle of incidence. A reduction from 10.1 ± 1.07 nm to 6 ± 1.02 nm was shown using an Ar beam at 1000 eV for 4 s at a 60° angle of incidence.

(Some figures in this article are in colour only in the electronic version)

1. Introduction

As the semiconductor industry tries to keep up with the trend of shrinking feature sizes in integrated circuits (IC) components, the line widths used in photoresists also continue to shrink. Even in the current 45 nm high-resolution node standard, more problems are still being addressed to keep the technology moving forward. According to the International Technology Roadmap for Semiconductors (ITRS), extreme ultraviolet (EUV) is the most likely light source for the next-generation lithography of semiconductors at the 22 nm half pitch node [1, 2]. However, before EUV lithography can be integrated into high volume manufacturing (HVM), several issues have to be resolved, including the reliability of the EUV light source, availability of defect-free masks, photoresist resolution and sensitivity, reflective mask protection during handling, the storage reliability of illuminator optics and line-edge roughness (LER) [3, 4]. One of the most significant areas of concern is that of LER. LER is any unwanted roughness in a semiconductor feature. In electron beam and EUV lithography, variations in the critical dimension (CD) due to the effect of shot-noise-related LER in too-sensitive resists should be given more consideration. This effect of LER is thus more critical in the spread in CD values at shorter line segment within the dimension such as the length of transistor gates [5, 6].

LER comes in two main varieties, short-wavelength and long-wavelength LER. Short-wavelength LER is mostly molecules left after development. Longer wavelength LER are undulations in the features caused by interference patterns and varying light strength. This will be increasingly important when lithography moves to EUV sources, as they have much less power than the excimer laser that is currently being used [7]. This LER is transferred through the processing steps and

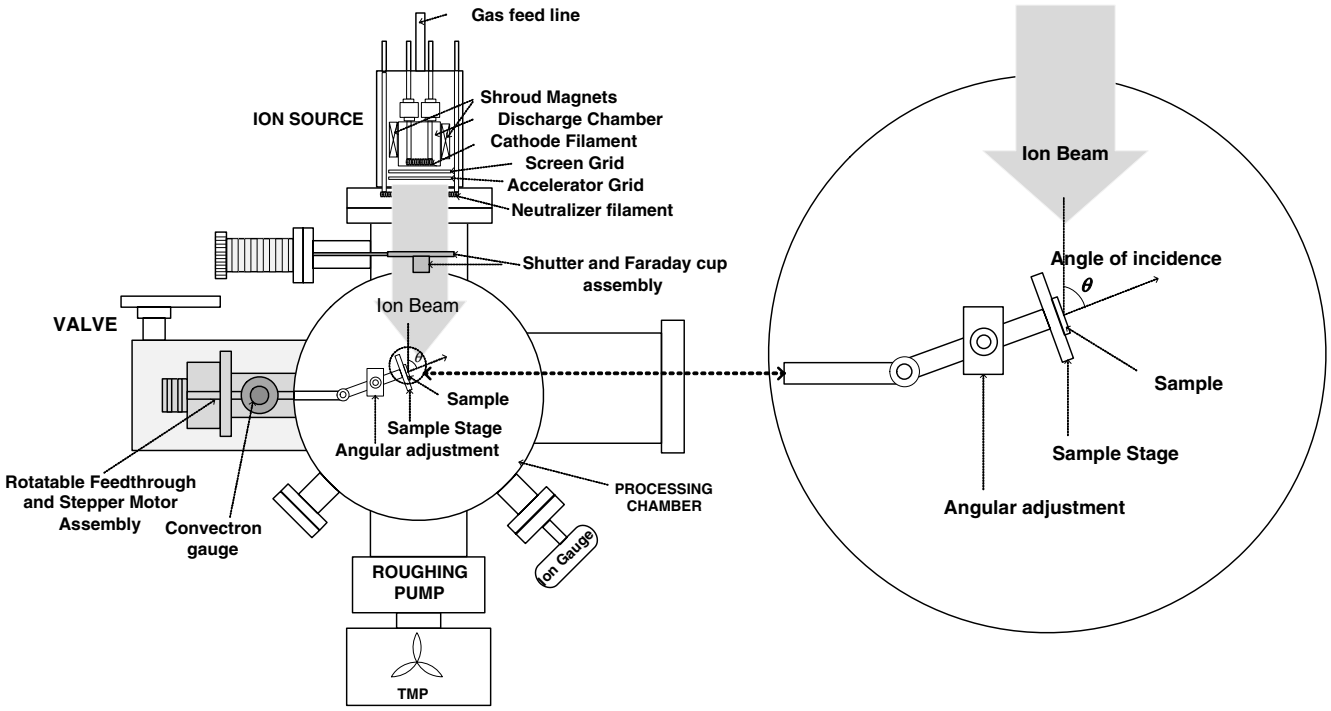

Figure 1. Schematic diagram of the LER reduction experimental facility.

makes components unreliable and prone to premature failure. If a molecule of photoresist shadows the trench while it is being etched for interconnect, the interconnect will have a thin region. The thin region will increase the current density in the interconnect leading to more heat production and increased electromigration. Thus, the LER reduction technique may be used as a post-processing step to reduce LER without significantly changing the CD while EUV source power and resist sensitivity are still sub-optimal. In this paper, an efficient and cost-effective way to reduce the LER in the semiconductor photoresist in order to keep the imperfections from processing steps further down the line is reported.

2. Experiments

The LER experimental setup at the Center for Plasma–Material Interactions (CPMI) consists of a gas-handling system, sample stage and a broad beam ion source. The gas flow into the chamber is controlled via a needle valve for precise control of process gases which can be finely tuned within the chamber by increments of 1×10^{-5} Torr. Gas flows from the source gas through a ball valve and then through a needle valve into the chamber. The gas is evacuated from the chamber using a Pfeifer TMU 071P turbomolecular pump backed by a Pfeifer MVP 015-2 or a Leybold Trivac D16A. The Trivac D16A has a N_2 volumetric flow rate of 6.65 l s^{-1}. The TMU 071P has a N_2 volumetric flow rate of 59 l s^{-1}. The Pfeifer MVP 015-2 is a diaphragm pump that has a volumetric flow rate of 0.31 l s^{-1}. These pumps allow for the chamber to have an ultimate pressure of 1×10^{-7} Torr.

A schematic diagram of the experimental setup is given in figure 1. The sample stage (with a blown-up image on the right-hand side of figure 1) consists of an angular adjustment mechanism connected to a rotatable feed-through and a programmable stepper motor. The angular adjustment mechanism can be used to control the angle of incidence of the ions within the chamber accurately. The angle is controlled by vertical posts which are threaded to allow for a slide control to move and be locked into place when the desired angle is achieved. Rotation is allowed throughout a large range of angles by a vacuum-compatible U-joint.

The setup is capable of rotating the sample at a specified angle of incidence with respect to the fixed beam direction. For each experiment, the sample was treated at one end and rotated 180° to process at the other end to provide uniform beam treatment on both ends. Thus, the beam treatment considered takes place when the sample was in its original angle with respect to the beam direction before the rotation and after rotation at 180°. Figure 2 shows the beam orientation to the sample and the sample features before rotation and after rotation at 90° and 180°, respectively. The sample stage is covered from the ion source by a shutter with an integrated Faraday cup as shown in figure 1. The shutter allows for beam warm-up for more precise process control. In this way, until the beam becomes stable, it is not hitting the sample. The Faraday cup integrated into the shutter provides greater reliability by knowing the ion flux every time a sample is processed. The presence of a Faraday cup also allows tuning of the ion beam to the same fluxes as before to prove repeatability.

For the LER reduction experiments, a 3 cm compact dc ion source from Veeco was used [8]. The ion source uses a radiantly cooled filament cathode that uses pyrolytic graphite grids for focusing and accelerating the ions. The ion source has a filament neutralizer to provide electrons to the sample and inhibit charging the sample and provide a more uniform

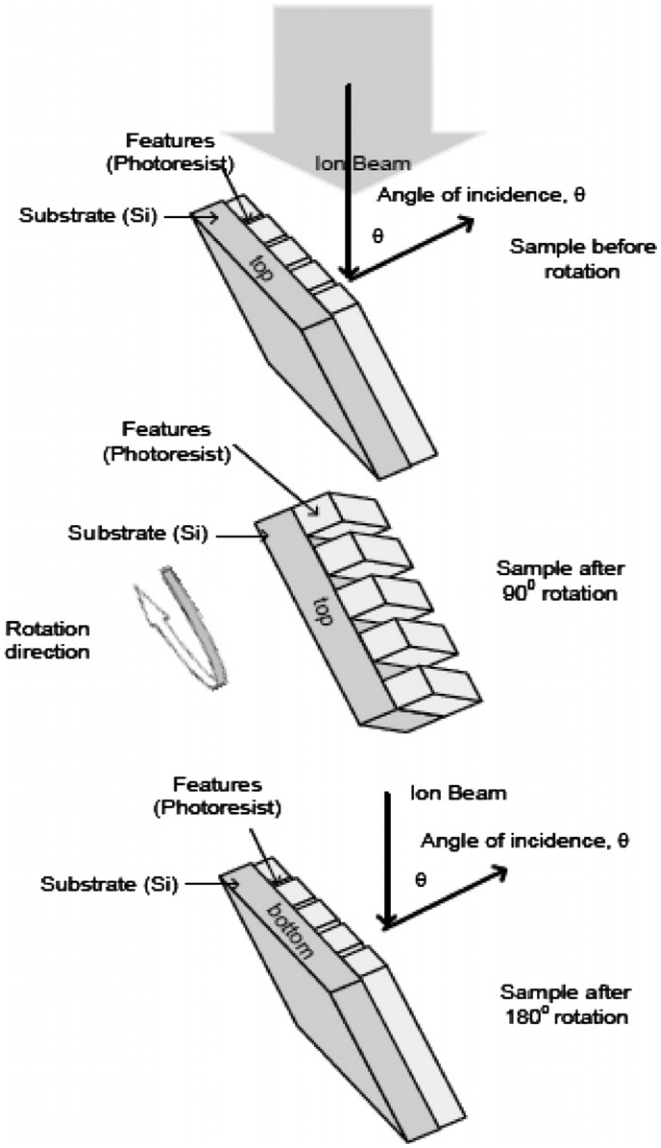

Figure 2. Orientation of the sample with respect to the fixed ion beam.

potential during ion beam operation. This source is capable of generating beam energies from 200 to 1200 eV allowing a wide range of experiments at different energies.

3. Results and discussion

3.1. Simulation results

Sputtering theory was used in the initial phase of this investigation to predict the removal of the projections on photoresist features without harming anything that might be underlying the feature. The features happen to be all aligned parallel with 45 nm 1:1 lines with an aspect ratio of 2:1. This allows the broad-beam ion source, once oriented, to hit the entire sample at once. The Stopping and Range of Ions in Matter (SRIM) simulations were conducted to give the 'relative' sputtering yield versus the angle of incidence but does not incorporate implantation effect near the surface

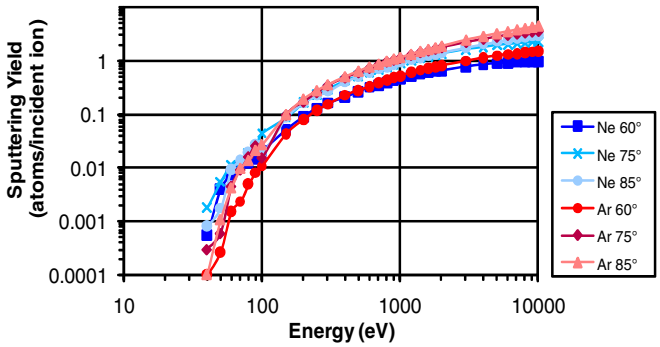

Figure 3. SRIM runs of sputtering coefficients of carbon versus energy for Ar and Ne [9].

region when ions are incorporated into the substrate during bombardment [9]. In this case, the SRIM simulation software was used to find the starting parameters, appropriate range of energies, angles of incidence, and to calculate the processing times.

From figure 3, it is seen that the photoresist follows the expected sputtering trend which showed increase in the sputtering yield as the ion energy is increased. At low energies, there is nothing sputtered, followed by a sharp rise in sputtering yield that finally knees into a more gradual rise in sputtering yield. The Yamamura formula [10] expands the Bohdansky [11, 12] formula to non-incident angles [13]. The Yamamura formula was also used to validate the SRIM results [9]. Although the angle of incidence of the ion beam can be adjusted at different angles in relation to the location of the sample, the sputtering yield showed optimum values within the angle of incidence range of 60–85° as shown in figure 4. Thus, the angles of incidence applied in our experiments were directed within this optimum range. The SRIM results show that carbon would be the atom limiting how fast the photoresist would sputter. Therefore, all time calculations were taken from carbon. Most of the photoresist must be left on the sample so the time to sputter only two to three monolayers was calculated. From this calculation, the processing time was determined for each combination of angle, energy and gas species used. It can be seen that at high angles of incidence, the sputtering rate increases. Using this as an advantage, any bump in the sidewall of the trench will have a greater time of beam interaction at larger incident angles and, hence, a greater chance of being hit by an energetic ion.

Argon and neon gas species were used in these experiments because they are noble gases and should have few, if any, chemical reactions with the photoresist. The angles of incidence chosen were 60°, 75° and 85°, within the optimal range based on the SRIM results. These angles were chosen due to their positions surrounding and close to the peak of the sputtering curve and also for their large cross-sectional area on the side of our features. Energies chosen for processing were 500 and 1000 eV with both gases and at all three angles. The different energies were chosen to see if there was any energy dependence besides the speed at which the photoresist would sputter.

Processing began on samples provided by Intel currently being used for the 45 nm technology node. These samples

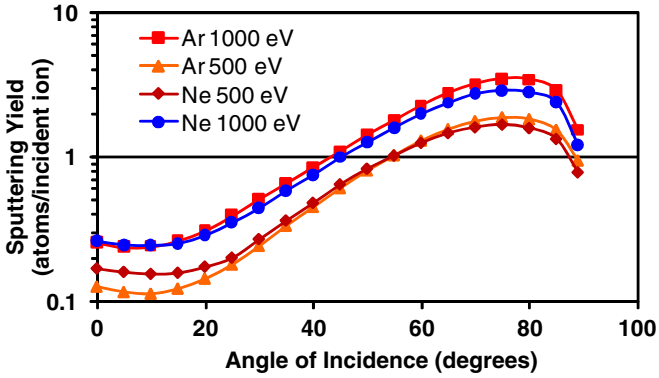

Figure 4. SRIM runs of sputtering coefficients of carbon versus angle for Ar and Ne [9].

are wafers that were spin coated with photoresist, printed using interference lithography with a flare to purposefully increase line-width roughness (LWR) in a pattern. Each wafer is divided into grids of 7 × 8 exposed sites. These sites were around 2 mm × 1 mm elliptical areas with features in them. These features were laid out in a grid-like pattern and aligned in the same direction. The photoresist was then developed so the features were revealed. Each wafer was then cleaved so that each exposed area becomes its own 1 cm × 1 cm sample. Since sputter coating and viewing a sample under a scanning electron microscope (SEM) change properties with the resist, as a comparison, a sample cleaved from directly next to the processed sample was used. While not allowing for a direct before and after comparison, this method allows for an unbiased comparison of a processed and an unprocessed sample. Six or more SEM images were taken randomly from the center of the exposed area in the photoresist. These images were than analyzed using Hitachi Online Terminal PC program. This program works by finding the contrast difference in the SEM images and extrapolating this into the edge of the feature.

3.2. Line-width roughness

For measurements used, the LWR feature in the Terminal PC software was utilized. LWR is the same as LER, but taken over both sides of the feature, instead of over just one side. The results from the Terminal PC program were then averaged by a sample to find out which combination of parameters had the best reduction in LWR. Figures 5(*a*) and (*b*) show the representative SEM images of an unprocessed and a processed sample. The unprocessed sample has a combined LWR value of 11.16 nm and the processed sample has a combined LWR value of 6.10 nm. This difference in the 3σ LWR value is a significant reduction when the goal is to have a 3σ value of less than 3 nm for the 45 nm node. The 3σ value represents three standard deviations from the mean. In this case, the mean is an extrapolated line through the middle of all of the edge points on the side of a feature [14].

To be able to provide statistical approach to our analyses, several images for each processed sample were measured. Shown in table 1 are raw sample data of the 3σ LWR

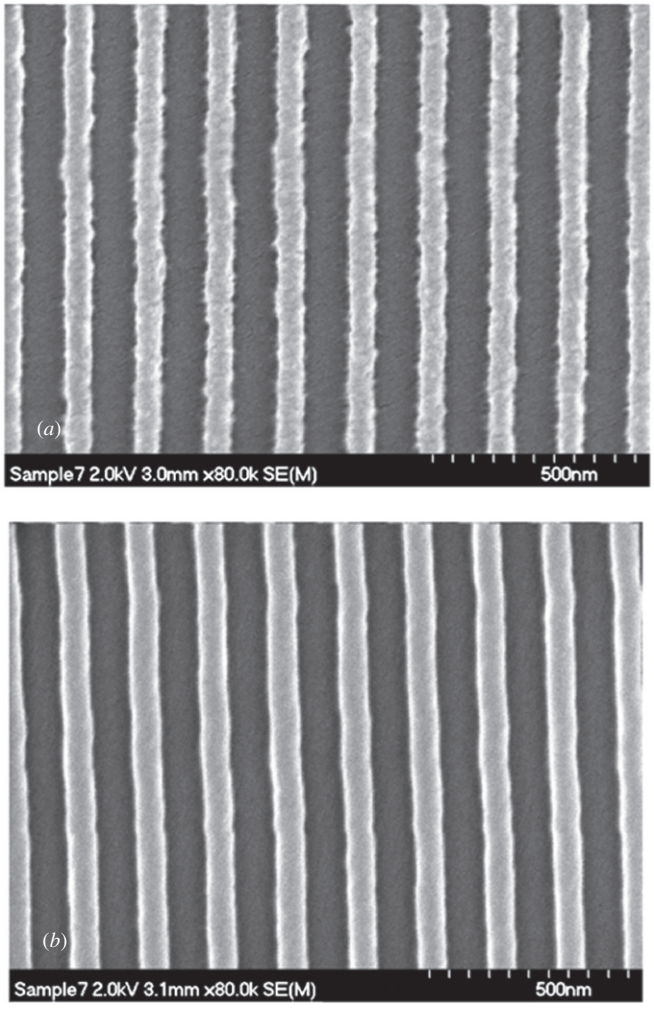

Figure 5. Representative SEM images of (*a*) the unprocessed sample and (*b*) the processed sample (b). The sample was processed with a 500 eV Ne beam at an 85° angle of incidence.

measurements for the unprocessed sample showing a mean of 9.8 nm and a standard deviation of 0.7 nm. The 3σ LWR values after processing are given in table 2 which shows an average LWR of 5.5 nm and a standard deviation of 0.9 nm. Note that 3σ' values are also shown for both processed and unprocessed tables. Sigma (σ) is just the standard deviation of the set of CDs measured at each point along a given line. Sigma prime (σ') is the same but with the maximum and minimum values thrown out—basically to allow for outliers where the line-edge fitting routine did not grab the right spot or where a particle landed on the edge of the line, etc. The 'Min – Max' is just the difference between the highest and lowest CD [14].

3.3. Fourier analysis

Another important part of the LWR analysis is the determination of the wavelength at which the roughness occurs. This can be determined through Fourier analysis of the output of the SEM image analysis. The shorter wavelength LWR (with a wavelength in the order of 10 nm) is attributed to molecules not being removed from the sidewall of the features.

Table 1. 3σ LWR for the unprocessed sample using Ne^+ at 500 eV and 85° angle of incidence.

Image number	3σ	$3\sigma'$	Min–Max
1	8.7	6.7	10.9
2	10.3	8.3	12.5
3	10.4	8.4	11.7
4	9.2	7.5	10.5
5	9.9	8.3	10.6
6	10.1	8	12.3
Mean	9.8	7.9	11.4
Standard deviation	0.7	0.7	0.9

Table 2. 3σ LWR for the processed sample using Ne^+ at 500 eV and 85° angle of incidence.

Image number	3σ	$3\sigma'$	Min – Max
1	4.2	3.6	4.7
2	5.6	4.5	6.6
3	5.9	4.5	7.4
4	6.8	5.1	8.2
5	5.1	4.1	5.8
6	5.4	4.5	6.2
Mean	5.5	4.4	6.5
Standard deviation	0.9	0.5	1.2

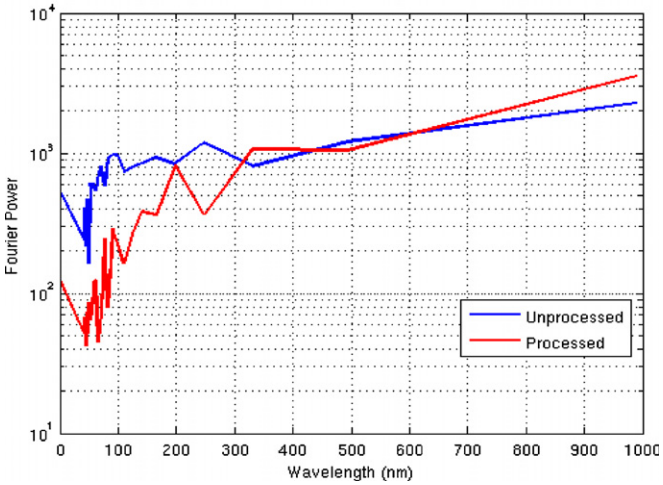

Figure 6. Power spectral density of the processed and unprocessed samples up to and including the wavelength of 980 nm. The intermediate and high spatial frequency roughness is reduced.

The long wavelength roughness (longer than 10 nm) comes from photoacid inhomogeneity in the photoresist along with interference patterns from the photolithography process. The results of the Fourier analysis for unprocessed and processed sample are shown in figures 6 (power spectral density versus wavelength) and 8 (LWR versus wavelength). As shown in figures 6 and 7, there was a reduction in the Fourier power at lower wavelength of 300 nm and below and an improvement in LWR across the spectrum from 50 nm to 1000 nm, respectively.

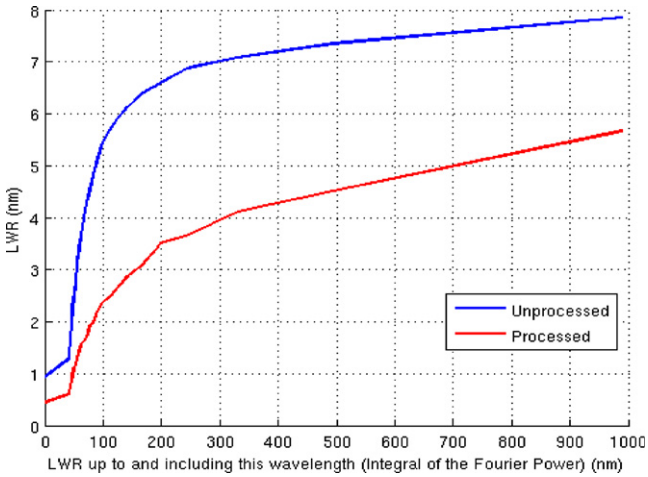

Figure 7. Fourier graph of the LWR up to and including the wavelength of 980 nm for the unprocessed and processed samples.

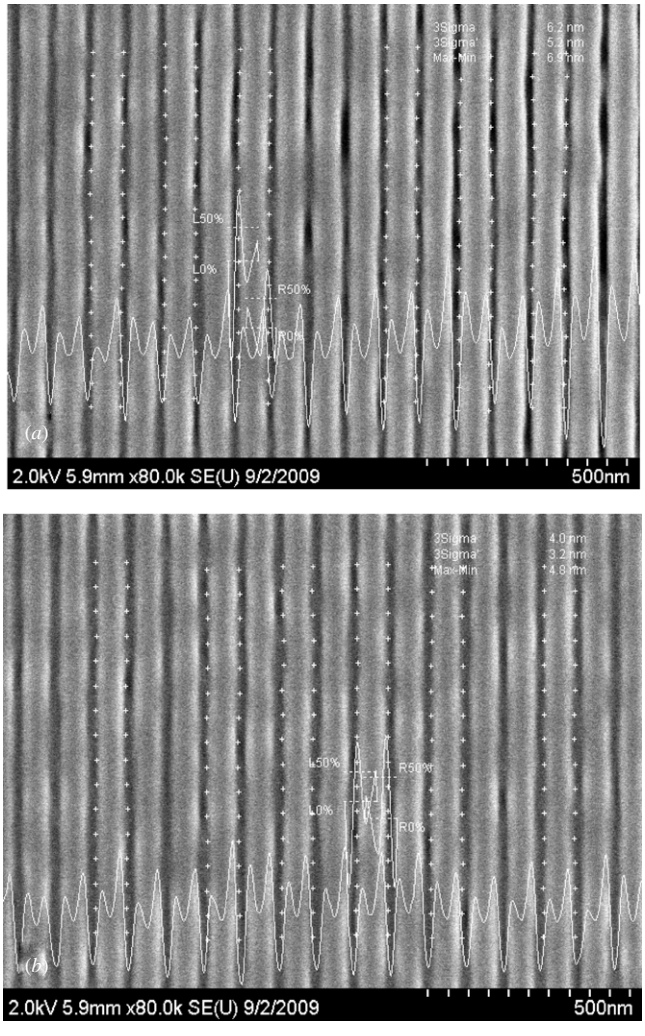

Figure 8. Representative SEM images of (*a*) the unprocessed sample and (*b*) the processed sample using EUV samples. The sample was processed with a 500 eV Ne beam at a 60° angle of incidence.

3.4. LER analysis using EUV samples

Representative samples from Intel developed by EUV lithography were also processed. These samples which are intended for the 22 nm node has a narrower gap width between patterns than the previous samples processed. The process gas

used was Ne at a pre-selected angle of 60° much lower the previous setting to minimize the change in the CD to within the allowable 4% change. Each sample cut from the wafer was laid out such that the pattern were aligned in the same direction and cleaved to produce processed and unprocessed samples coming in from the same EUV spot. In this case, the samples were imaged using SEM without sputter coating. For each sample, 12 images were taken randomly to provide a reliable statistical comparison. In figures 8(*a*) and (*b*) representative images of both processed and unprocessed samples are shown. While the two samples do not look much different, their LWR numbers are significantly different. The LER of the unprocessed sample is 5.35 ± 0.24 with a CD width of 72.3 ± 3.5. After processing of 30 s for each side, the processed samples showed a LER of 4.44 ± 0.18 and a CD width of 72.2 ± 2.1, corresponding to a 17% LER reduction with only 0.1% CD width change.

4. Conclusions

The removal of LER from a patterned photoresist using an ion beam at grazing angles of incidence has been found to be successful. The SRIM/TRIM simulation provided the sputtering yield calculation for both Ar and Ne. SRIM/TRIM simulations showed an increased sputtering rate at higher angles of incidence. Both argon and neon were used as gas species at energies of 500 and 1000 eV and at angles of 60°, 75° and 85°. These results showed that it is possible to significantly reduce the LWR of photoresist from all wavelengths using this technique.

Acknowledgments

The authors would like to thank Intel for providing the samples and funding under Inter SRA 03-159. They also thank Tim Grunloh, an undergraduate research assistant, for experimental help. SEM imaging was carried out at the Frederick Seitz Materials Research Laboratory (FS-MRL) of the University of Illinois at Urbana-Champaign, which are partially supported by the US Department of Energy under grants DE-FG02-07ER46453 and DE-FG02-07ER46471, and the Micro and Nanotechnology Laboratory at the University of Illinois Urbana-Champaign.

References

[1] ITRS 2008 *International Technology Roadmap for Semiconductors* http://www.net/Links/2007ITRS/2007 Chapters/2007
[2] Wurm S 2008 *EUVL Symposium Closing Address, Int. EUVL Symp. (Lake Tahoe, 2008)*
[3] Ruzic D N and Srivastava S N 2008 Collector contamination: normal incidence (multilayer) collectors *EUV Lithography* ed V K Bakshi (Bellingham, WA: SPIE)
[4] Rice B J, Cao H, Chandhok M and Meagley R 2003 Effects of processing parameters on line width roughness *Proc. SPIE* **5039** 384–92
[5] Kruit P and Steenbrink S 2005 Local critical dimension variation from shot-noise related line edge roughness *J. Vac. Sci. Technol.* B **23** 3033–6
[6] Yamaguchi A *et al* 2004 *Proc. SPIE* **5375** 468
[7] Thompson K C *et al* 2006 *Microelectron. Eng.* **83** 476–84
[8] Veeco Instruments 2007 Veeco 3 cm DC Ion Source
[9] Ziegler J F, Ziegler M D and Biersack J P 2006 Stopping Power and Range of Ions in Matter (SRIM)
[10] Matsunami N, Yamamura Y, Itikawa Y and Itoh N 1983 *Report IPPJ-AM-32* (Nagoya: Institute of Plasma Physics, Nagoya University)
[11] Bohdansky J 1984 *Nucl. Instrum. Methods Phys. Res.* B **2** 587–91
[12] Eckstein W *et al* 1993 *IPP Report IPP 8/82* (Garching: Max-Planck-Institut für Plasmaphysik)
[13] Smith P C and Ruzic D N 1998 *Nucl. Fusion* **38** 673–80
[14] Hitachi High-Tech Science Systems Corporation 2007 *Instruction Manual: Terminal PC Online CD Measurement Software (v5.04) for Hitachi CD Measurement and Evaluation SEM*